Long-Range Alignment of Gold Nanorods in Electrospun Polymer Nano/Microfibers

Kristen E. Roskov,[†] Krystian A. Kozek,[‡] Wei-Chen Wu,[‡] Raghav K. Chhetri,[§] Amy L. Oldenburg,[§] Richard J. Spontak,[†,‡] and Joseph B. Tracy*,[‡]

[†]Department of Chemical & Biomolecular Engineering and [‡]Department of Materials Science & Engineering, North Carolina State University, Raleigh, North Carolina 27695, United States
[§]Department of Physics & Astronomy, University of North Carolina, Chapel Hill, North Carolina 27599, United States

S *Supporting Information*

ABSTRACT: In this study, a scalable fabrication technique for controlling and maintaining the nanoscale orientation of gold nanorods (GNRs) with long-range macroscale order has been achieved through electrospinning. The volume fraction of GNRs with an average aspect ratio of 3.1 is varied from 0.006 to 0.045 in aqueous poly(ethylene oxide) solutions to generate electrospun fibers possessing different GNR concentrations and measuring 40−3000 nm in diameter. The GNRs within these fibers exhibit excellent alignment with their longitudinal axis parallel to the fiber axis *n*. According to microscopy analysis, the average deviant angle between the GNR axis and *n* increases modestly from 3.8 to 13.3° as the fiber diameter increases. Complementary electron diffraction measurements confirm preferred orientation of the {100} GNR planes. Optical absorbance spectroscopy measurements reveal that the longitudinal surface plasmon resonance bands of the aligned GNRs depend on the polarization angle and that maximum extinction occurs when the polarization is parallel to *n*.
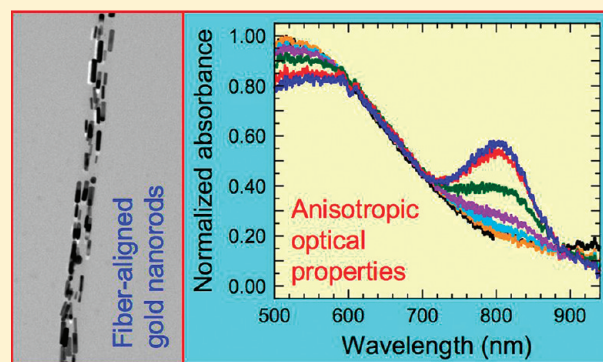
Nanoparticle (NP) synthesis, characterization, and self-assembly have been thoroughly investigated over the past two decades primarily because of their novel size- and shape-tunable functional properties,[1] as well as the wide variety of property enhancements they impart to matrix materials such as polymers.[2] As their size decreases, metal NPs can exhibit physical and chemical properties (e.g., catalytic,[3] optical,[4] electronic,[5] and magnetic[6]) that are not observed in the bulk. Gold and silver NPs, for instance, are known to exhibit strong surface plasmon resonances in the visible electromagnetic spectrum as a consequence of optically driven coherent oscillations of conduction electrons.[7] These resonances give rise to characteristic optical absorption and scattering spectra,[8] yielding brightly colored, NP-containing suspensions. Gold nanorods[9] (GNRs) have recently attracted considerable attention because of their strong and uniquely tunable longitudinal surface plasmon resonance (LSPR) along the longitudinal GNR axis. The LSPR wavelength of GNRs can be adjusted from ∼520 nm in the case of low-aspect-ratio (i.e., spherical) gold NPs to at least 1750 nm in the near-infrared region of the electromagnetic spectrum for high-aspect-ratio GNRs.[10] Currently, GNRs with an LSPR at 800 nm are of particularly significant interest for *in vivo* imaging of biological systems because blood and tissue exhibit an absorbance minimum at this wavelength.[11−13]

When dispersed in a solvent, GNRs are randomly oriented, and they tend to remain so when physically deposited on surfaces. If the distribution of GNR sizes and shapes is sufficiently narrow

such that the GNRs can be considered to be nearly monodisperse, they can spontaneously self-assemble into ordered grains with different orientations.[14,15] Presently, the alignment of such grains over macroscale dimensions is a significant technological challenge, but is highly desirable[16] because the optical anisotropy[17] of GNRs evaluated at the LSPR can be greater than ∼250:1.[18] A scalable method for controlling and maintaining the orientation of GNRs on the nanoscale while fabricating macroscale structures that exploit GNR orientation is therefore needed to create nanostructured composites with tunable, anisotropic optical properties. Alignment-enhanced absorption of polymer/GNR composites has been previously reported using different preparation strategies: thin-film stretching,[19−22] block-copolymer-templated organization,[23,24] directed nanoscale assembly,[25,26] ultrathin film confinement,[27] and polymer fiber coating.[28] An ongoing challenge for polymer/GNR composites produced by these methods is the consistent acquisition of long-range, scalable order of highly aligned GNRs along a common axis (rather than randomly oriented in a common plane). Here, we describe a general technique for aligning GNRs within electrospun polymer nano/microfibers with diameters ranging from 40 to 3000 nm. Our approach enables the hierarchical alignment of fibers containing aligned nanorods over large, macroscopic dimensions.
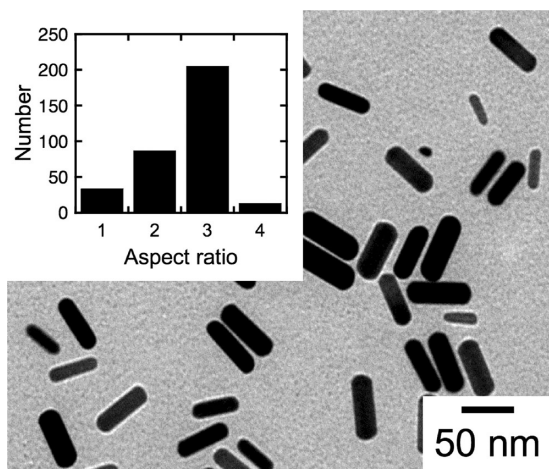
Figure 1. TEM image of GNRs deposited from an aqueous suspension onto a carbon-coated TEM grid. The inset shows the distribution of the measured aspect ratios of the GNRs, which measure 49 nm long and 17 nm in diameter on average.
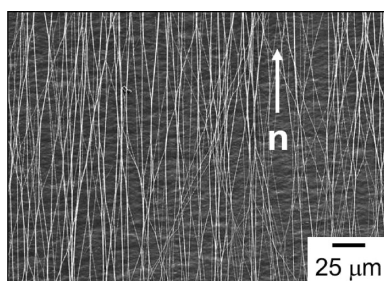
Figure 2. SEM image of macroscopically aligned electrospun PEO fibers containing GNRs.

The resultant polymer/GNR composites are characterized by electron microscopy, electron diffraction, and optical absorbance spectroscopy.

The GNRs investigated here were synthesized by modifying a method originally introduced by Nikoobakht et al.[29] Details of the GNR synthesis are provided as Supporting Information. A custom-built electrospinning unit with an Al collection target was operated at an electric potential of 10 kV with a plate distance of 15 cm and flow rates of 30−50 μL/min. Aligned electrospun fibers, rather than conventional, randomly oriented fiber mats, were generated by electrospinning between two grounded electrodes separated by 2 cm.[30] Prior to electrospinning, the GNR stock suspension was warmed with a heat gun to redissolve precipitated cetyltrimethylammonium bromide (CTAB). Poly-(ethylene oxide) (PEO: 1000 kDa, Sigma-Aldrich) was selected for its intrinsic hydrophilicity and, by inference, its compatibility with the native CTAB coating on the GNRs. A high-molecular-weight grade was chosen to facilitate fiber formation and impart mechanical robustness (for handling purposes). Although other matrix materials have not yet been explored, we anticipate that similar results would be obtained for comparably water-soluble polymers amenable to electrospinning. The PEO was dissolved directly into the GNR stock suspension to yield a maximum GNR volume fraction (Φ) of 0.045. Lower GNR volume fractions were subsequently prepared by first dissolving the polymer in a separate deionized

water solution and then adding it to the GNR suspension. Polymer concentrations ranged from 3.0 to 4.5 wt % PEO. Immediately before electrospinning, the mixture was sonicated for 10 min to ensure a uniform GNR dispersion. Electrospun fibers were dried under vacuum for 24 h at ambient temperature.

Specimens imaged by transmission electron microscopy (TEM) consisted of randomly oriented fibers electrospun directly onto carbon-coated Cu grids. Images and selected-area electron diffraction (SAED) patterns were acquired on a field-emission Hitachi HF2000 microscope operated at 200 kV. Corresponding scanning electron microscopy (SEM) images were collected from specimens sputter-coated with 6 nm of Au/Pd on a JEOL 6400F field-emission microscope operated at 5 kV. For optical characterization, a custom-built polarized UV−vis spectrophotometer housing a fiber-coupled white-light source (Photon Control), broadband linear polarizer, light collection fiber coupled to a USB spectrometer (Lightspeed Technologies), and a series of collimation and collection lenses was employed. Absorbance spectra were acquired by orienting each specimen normal to the collimated white-light beam, which was passed through an aperture measuring ~2 mm in diameter and the polarizer.

The GNRs employed in this study have an average width and length of 17 ± 6 and 49 ± 10 nm, respectively (Figure 1), which results in an average aspect (length/diameter) ratio of 3.1. Electrospinning is becoming established as an important method of preparing polymer nano/microfibers because it is straightforward to perform and offers the flexibility to tune fiber characteristics by controllably varying specimen and/or processing parameters. Aligned fibers generated by electrospinning between two grounded electrodes yield a freestanding, oriented mat measuring 10 cm wide and 3 cm or more long (Figure 2). Here and in subsequent discussion, n refers to the fiber axis direction. The fiber thickness is governed by the PEO concentration when all other electrospinning parameters are held constant. For instance, the nanofibers shown in Figure 3a with an average diameter of ~40 nm were electrospun from an aqueous suspension with Φ = 0.006 and a PEO concentration of 3.2 wt %. At this relatively low GNR loading in PEO nanofibers, the GNRs orient with their longitudinal axis parallel to n. To quantify the extent of alignment along n, the average deviant angle ($\langle\theta_{dev}\rangle$) determined from the angular difference between the GNR orientation and n has been measured for 150−300 GNRs embedded within electrospun PEO fibers of varying thickness. For nanofibers such as those shown in Figure 3a, $\langle\theta_{dev}\rangle$ = 3.8°. Very few GNR aggregates are observed at this low loading level, for which the interparticle distance is typically much longer than the length of the GNR. The theory proposed by Bates and Frenkel[31] for hard-rod fluids predicts that GNRs with aspect ratios of <7 should exhibit random orientation in suspension, insofar as the GNRs do not interact with each other over large distances. According to our observations, it follows that oriented, well-separated GNRs, for instance, in Figure 3a are aligned by forces other than those arising from interparticle interactions.
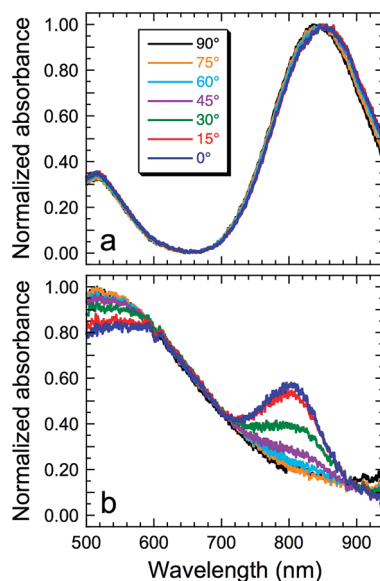
During electrospinning, the viscous polymer/GNR suspension at the tip of the syringe can be modeled[32] as a fluid cone leading to a jet, where the charged liquid is emitted. Sink-like flow emerges at the apex of the cone, and streamlines form due to the rapid decrease in area. In suspensions, the GNRs are initially randomly oriented but begin to align along the streamlines leading to the jet. Because the Reynolds number, defined as the ratio of inertial (drag) to viscous forces, is much less than unity at this point, the translational velocity component dominates,[33] in which case the
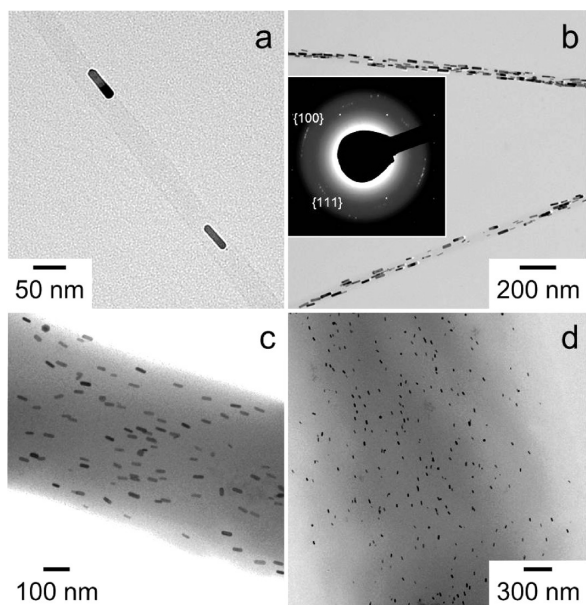
Figure 3. Aligned GNRs in electrospun PEO nano/microfibers as respective functions of fiber diameter and GNR volume fraction (Φ): (a) 40 nm and $\Phi = 0.006$, (b) 50 nm and $\Phi = 0.045$, (c) 650 nm and $\Phi = 0.035$, and (d) 3000 nm and $\Phi = 0.031$. A selected-area electron diffraction pattern of the corresponding sample is included as an inset in (b).

Figure 4. Absorbance spectra for (a) randomly oriented GNRs in a PEO film measuring ~500 μm thick at different polarization angles and (b) GNRs aligned within electrospun PEO microfibers measuring ~200 nm in diameter at polarization angles varying from 0° (parallel to the fiber axis *n*) to 90° (perpendicular to *n*). In both cases, the data are color coded and labeled in plot (a).

center of each GNR experiences the same velocity as the local fluid velocity. As the viscoelastic liquid leaves the jet, the GNRs are expected to be oriented for the most part along the fiber spinning direction. Indeed, the alignment of significantly longer carbon nanotubes[34] and CdS nanorods with an aspect ratio of ~20[35] has been experimentally confirmed in electrospun fibers, but we are unaware of prior studies of aligned nanorods with shorter aspect ratios within electrospun fibers. When the GNR loading is increased to $\Phi = 0.045$ (Figure 3b), the GNRs remain highly oriented because their orientation is predominately dictated by the local velocity profile. For an increased fiber diameter of ~650 nm and $\Phi = 0.035$ (Figure 3c), the velocity profile is forced to extend across the diameter of the microfiber. Consequently, the GNR longitudinal axes remain highly aligned with *n*, but $\langle\theta_{dev}\rangle$ increases modestly to 8.8°. When the fiber diameter is further increased to ~3000 nm and $\Phi = 0.031$ (Figure 3d), the degree of GNR alignment decreases, as verified by an accompanying increase in $\langle\theta_{dev}\rangle$ to 13.3°.

Two other key morphological observations warrant mention. The first is that long GNRs are more highly oriented with respect to *n* than are short ones. For example, in a fiber measuring ~80 nm in diameter, when measurements of $\langle\theta_{dev}\rangle$ are sorted according to the GNR length, the shortest 26% of the GNRs possess a $\langle\theta_{dev}\rangle$ value that is 54% greater than $\langle\theta_{dev}\rangle$ for all GNRs in the fiber. Second, the fiber diameter is one of the main factors that determine the degree of GNR alignment within electrospun fibers. That is, within fibers of nearly constant diameter, the extent of alignment does not appear to depend strongly on Φ over the range of GNR concentrations investigated. These two results imply that the degree of nanoscale GNR orientation over macroscale dimensions is primarily controlled by the flow field introduced by the polymer and experienced by the GNRs during electrospinning, coupled with the GNR aspect ratio.

Performing SAED on a segment of microfiber measuring 200 nm in diameter and containing ~20 GNRs yields the pattern included as an inset in Figure 3b. Previous studies have shown that GNRs possess a faceted crystal structure with a $[110]$ growth direction, $\{111\}$ end facets, and $\{100\}$ side facets.[36,37] Analysis of the SAED pattern in Figure 3b confirms the existence of a face-centered cubic lattice with preferred orientations identified by the $\{100\}$ reflections, which is consistent with results reported elsewhere.[14] These reflections appear over a limited angular range rather than as single spots, which indicates a distribution of GNR orientations. This result has been analyzed in terms of the truncated Hermans orientation function (P_2),[38] written as

$$P_2 = \frac{3\langle\cos^2\phi\rangle - 1}{2} \tag{1}$$

Here, ϕ is the azimuthal angle extending from 0 to 2π around the circular SAED pattern, and

$$\langle\cos^2\phi\rangle = \frac{\int I(\phi)\cos^2(\phi)\,d\phi}{\int I(\phi)\,d\phi} \tag{2}$$

where $I(\phi)$ is the intensity that varies along a circular trace of constant radius. Limiting values of P_2 are 1.0 for perfect alignment along *n*, 0.0 for random dispersions, and −0.5 for perpendicular alignment relative to *n*. The present analysis yields $P_2 = 0.73$ for the aligned GNR-containing PEO microfibers under investigation, which further confirms that the GNRs are highly oriented within the microfibers.

Gold nanorods are of particular contemporary interest because of their anisotropic optical properties. To observe the optical anisotropy of an ensemble of GNRs, alignment of the GNRs is required. Furthermore, oriented GNRs may have controllable end-to-end coupling between their LSPRs (in contrast to the

distribution of relative orientations found in isotropic dispersions of GNRs),[39] especially at high GNR loading levels. Several independent reports of the optical properties of GNRs aligned with electric fields[40] or in stretched polymers[19−22] have established that linearly polarized light oriented with the electric field parallel to the GNR long axis excites the LSPR but does not excite the transverse surface plasmon. Here, we show similar results for aligned GNRs in oriented electrospun PEO microfibers.

Optical absorbance spectra have been collected using the custom-built UV−vis spectrophotometer described earlier. As a benchmark, spectra acquired at different polarization angles from GNRs randomly dispersed in a PEO film measuring ~500 μm thick are presented in Figure 4a and reveal the existence of clearly discernible and angle-independent LSPR peaks near ~520 and ~850 nm. These signature features are likewise observed for GNRs dispersed in water, confirming that the bulk, semicrystalline PEO has little effect on GNR orientation. The absorbance spectra of aligned GNRs in electrospun PEO microfibers measuring 200 nm in diameter (Figure 4b) strongly depend on the polarization angle. As expected, the LSPR peak at 804 nm is most pronounced when the polarizer is parallel to n (and to the GNR longitudinal axis) at 0° but vanishes when the polarizer is perpendicular to n at 90°. Similarly, the absorbance in the 500−600 nm region decreases when the polarizer is parallel to n at 0° because the transverse surface plasmon is not excited. The position of the LSPR peak indicates a red shift of 40 nm relative to a random GNR dispersion in water (cf. Figure S-1 in the Supporting Information). The analogous LSPR peak in the random dispersion of GNRs in a PEO film is centered at 847 nm (Figure 4a), which corresponds to a further red shift of ~40 nm. Shifts in the LSPR wavelength may arise from several sources, such as interparticle coupling,[41,42] differences between the refractive indices of PEO and water, and the crystallinity of PEO.

The absorbance spectra in Figure 4b have been processed to remove background contributions from the glass substrate and from the optical scattering of the polymer fibers. Spectra for the GNR-containing and control fiber specimens prior to subtraction are included for examination in Figure S-2 of the Supporting Information. In contrast to polymer thin films, polymer fibers contribute a scattering signal to the total extinction that is significantly greater than the extinction of the GNRs, which results in noisier absorbance spectra from the oriented GNRs in fibers. All spectra are smoothed using a 17-point Savitzky−Golay numerical procedure.[43] An aligned PEO microfiber mat without GNRs is selected as an appropriate control specimen for Figure 4b. The difference in specimen density accompanying the incorporation of GNRs is taken into account by Beer's law

$$A = \mu z \qquad (3)$$

where A denotes the absorbance, μ is the extinction coefficient, and z is the specimen thickness. In Figure 4a, the absorbance spectra of randomly dispersed GNRs in a PEO thin film display a minimum near 650 nm. It immediately follows that $\mu_{GNR} \approx \mu_c$ at this wavelength, thereby yielding $A_{GNR}/z_{GNR} \approx A_c/z_c$, where the subscripted c represents the control specimen without GNRs. The thicknesses of the control and GNR-containing specimens can therefore be related by their absorbance values at 650 nm, and control spectra have been subtracted from the spectrum for the GNR-containing fibers. After this correction, the spectra are normalized to zero and unity. We note, however, that $\mu_{GNR} > \mu_c$ at 650 nm because the GNRs have a small, but nonzero,

absorbance at 650 nm. Consequently, the background correction in Figure 4b does not completely remove spectral contributions originating from polymer fiber scattering, which is responsible for the downward slope in the baseline over ~~600−700 nm. The optical anisotropy of the GNRs could be further increased by improving the alignment of the GNRs within the polymer microfibers and the parallel orientation of the microfibers.

In conclusion, we have demonstrated a scalable method for controlling and maintaining the nanoscale orientation of GNRs with long-range macroscopic order over a distance of several centimeters. Here, GNRs with an aspect ratio of 3.1 exhibit excellent alignment with their longitudinal axes parallel to n for electrospun polymer nano/microfibers with diameters of 40−600 nm, and they maintain substantial alignment in microfibers measuring up to 3000 nm in diameter. Whereas the fiber diameter is found to play a crucial role in GNR alignment, GNR concentration can be varied with no discernible impact on the net degree of alignment. Electron diffraction measurements of the aligned GNRs confirm the preferred orientation of the {100} GNR planes. Optical absorbance spectroscopy measurements performed on microscopically aligned GNRs in macroscopically aligned electrospun fibers demonstrate that the LSPR bands are polarization-dependent and display maximum extinction when the polarizer is parallel to n.

■ ASSOCIATED CONTENT

ⓢ **Supporting Information.** Synthesis procedure for the GNRs employed here, their optical absorbance spectrum in water, and additional spectra of GNR-containing and control fiber specimens. This material is available free of charge via the Internet at http://pubs.acs.org.

■ ACKNOWLEDGMENT

■ REFERENCES

(1) Tao, A. R.; Habas, S.; Yang, P. D. *Small* **2008**, *4*, 310–325.
(2) Merkel, T. C.; Freeman, B. D.; Spontak, R. J.; He, Z.; Pinnau, I.; Meakin, P.; Hill, A. J. *Science* **2002**, *296*, 519–522.
(3) Sun, Y. G.; Xia, Y. N. *Science* **2002**, *298*, 2176–2179.
(4) Barnes, W. L.; Dereux, A.; Ebbesen, T. W. *Nature* **2003**, *424*, 824–830.
(5) Schön, G.; Simon, U. *Colloid Polym. Sci.* **1995**, *273*, 101–117.
(6) Whitney, T. M.; Jiang, J. S.; Searson, P. C.; Chien, C. L. *Science* **1993**, *261*, 1316–1319.
(7) Kelly, K. L.; Coronado, E.; Zhao, L. L.; Schatz, G. C. *J. Phys. Chem. B* **2003**, *107*, 668–677.
(8) Link, S.; El-Sayed, M. A. *J. Phys. Chem. B* **1999**, *103*, 8410–8426.
(9) Murphy, C. J.; Thompson, L. B.; Chernak, D. J.; Yang, J. A.; Sivapalan, S. T.; Boulos, S. P.; Huang, J.; Alkilany, A. M.; Sisco, P. N. *Curr. Opin. Colloid Interface Sci.* **2011**, *16*, 128–134.
(10) Jana, N. R.; Gearheart, L.; Murphy, C. J. *J. Phys. Chem. B* **2001**, *105*, 4065–4067.
(11) Weissleder, R. *Nat. Biotechnol.* **2001**, *19*, 316–317.
(12) Oldenburg, A. L.; Hansen, M. N.; Ralston, T. S.; Wei, A.; Boppart, S. A. *J. Mater. Chem.* **2009**, *19*, 6407–6411.

(13) Durr, N. J.; Larson, T.; Smith, D. K.; Korgel, B. A.; Sokolov, K.; Ben-Yakar, A. *Nano Lett.* **2007**, *7*, 941–945.

(14) Nikoobakht, B.; Wang, Z. L.; El-Sayed, M. A. *J. Phys. Chem. B* **2000**, *104*, 8635–8640.

(15) Sau, T. K.; Murphy, C. J. *Langmuir* **2005**, *21*, 2923–2929.

(16) Vaia, R. A.; Maguire, J. F. *Chem. Mater.* **2007**, *19*, 2736–2751.

(17) Sönnichsen, C.; Alivisatos, A. P. *Nano Lett.* **2005**, *5*, 301–304.

(18) Chhetri, R. K.; Kozek, K. A.; Johnston-Peck, A. C.; Tracy, J. B.; Oldenburg, A. L. *Phys. Rev. E* **2011**, *83*, 040903.

(19) van der Zande, B. M. I.; Pagès, L.; Hikmet, R. A. M.; van Blaaderen, A. *J. Phys. Chem. B* **1999**, *103*, 5761–5767.

(20) Pérez-Juste, J.; Rodríguez-González, B.; Mulvaney, P.; Liz-Marzán, L. M. *Adv. Funct. Mater.* **2005**, *15*, 1065–1071.

(21) Murphy, C. J.; Orendorff, C. J. *Adv. Mater.* **2005**, *17*, 2173–2177.

(22) Li, J. F.; Liu, S. Y.; Liu, Y.; Zhou, F.; Li, Z. Y. *Appl. Phys. Lett.* **2010**, *96*, 263103.

(23) Deshmukh, R. D.; Liu, Y.; Composto, R. J. *Nano Lett.* **2007**, *7*, 3662–3668.

(24) Nie, Z. H.; Fava, D.; Kumacheva, E.; Zou, S.; Walker, G. C.; Rubinstein, M. *Nat. Mater.* **2007**, *6*, 609–614.

(25) Sánchez-Iglesias, A.; Grzelczak, M.; Pérez-Juste, J.; Liz-Marzán, L. M. *Angew. Chem., Int. Ed.* **2010**, *49*, 9985–9989.

(26) Correa-Duarte, M. A.; Pérez-Juste, J.; Sánchez-Iglesias, A.; Giersig, M.; Liz-Marzán, L. M. *Angew. Chem., Int. Ed.* **2005**, *44*, 4375–4378.

(27) Hore, M. J. A.; Composto, R. J. *ACS Nano* **2010**, *4*, 6941–6949.

(28) Chang, H. L.; Tian, L.; Abbas, A.; Kattumenu, R.; Singamaneni, S. *Nanotechnology* **2011**, *22*, 275311.

(29) Nikoobakht, B.; El-Sayed, M. A. *Chem. Mater.* **2003**, *15*, 1957–1962.

(30) Li, D.; Wang, Y. L.; Xia, Y. N. *Nano Lett.* **2003**, *3*, 1167–1171.

(31) Bates, M. A.; Frenkel, D. *J. Chem. Phys.* **2000**, *112*, 10034–10041.

(32) Yarin, A. L.; Koombhongse, S.; Reneker, D. H. *J. Appl. Phys.* **2001**, *90*, 4836–4846.

(33) Forest, M. G.; Zhou, R. H.; Wang, Q. *Int. J. Numer. Anal. Mod.* **2007**, *4*, 478–488.

(34) Dror, Y.; Salalha, W.; Khalfin, R. L.; Cohen, Y.; Yarin, A. L.; Zussman, E. *Langmuir* **2003**, *19*, 7012–7020.

(35) Bashouti, M.; Salalha, W.; Brumer, M.; Zussman, E.; Lifshitz, E. *ChemPhysChem* **2006**, *7*, 102–106.

(36) Johnson, C. J.; Dujardin, E.; Davis, S. A.; Murphy, C. J.; Mann, S. *J. Mater. Chem.* **2002**, *12*, 1765–1770.

(37) Petrova, H.; Perez-Juste, J.; Zhang, Z. Y.; Zhang, J.; Kosel, T.; Hartland, G. V. *J. Mater. Chem.* **2006**, *16*, 3957–3963.

(38) Hermans, J. J.; Hermans, P. H.; Vermaas, D.; Weidinger, A. *Recl. Trav. Chim. Pays-Bas* **1946**, *65*, 427–447.

(39) Wang, Y.; DePrince, A. E.; Gray, S. K.; Lin, X. M.; Pelton, M. *J. Phys. Chem. Lett.* **2010**, *1*, 2692–2698.

(40) van der Zande, B. M. I.; Koper, G. J. M.; Lekkerkerker, H. N. W. *J. Phys. Chem. B* **1999**, *103*, 5754–5760.

(41) Jain, P. K.; Eustis, S.; El-Sayed, M. A. *J. Phys. Chem. B* **2006**, *110*, 18243–18253.

(42) Vial, S.; Pastoriza-Santos, I.; Pérez-Juste, J.; Liz-Marzán, L. M. *Langmuir* **2007**, *23*, 4606–4611.

(43) Savitzky, A.; Golay, M. J. E. *Anal. Chem.* **1964**, *36*, 1627–1639.